Cellulose (2020) 27:157–170
https://doi.org/10.1007/s10570-019-02809-y

ORIGINAL RESEARCH

Quantitative Raman spectroscopy for the Ioncell^{TM} process. Part 1: comparison of univariate and multivariate calibration methods for the quantification of water and protic ionic liquid components

Chamseddine Guizani · Sanna Hellstén · Joanna Witos · Herbert Sixta

Received: 16 July 2019 / Accepted: 21 October 2019 / Published online: 2 November 2019

Abstract We investigate in this paper the potential of Raman spectroscopy for the quantification of protic ionic liquid components (acid and base) and water, in ionic liquid/water mixtures, taking 1.5-Diazabicyclo[4.3.0]non-5-enium acetate ([DBNH][OAc]) as a case study. We show that the combination of Raman spectroscopy and chemometrics is quite successful for the quantitative analysis of the ionic liquid components and water in mixtures over wide concentration ranges. The finding of the present work suggest that Raman spectroscopy should be considered more universally for the in-line monitoring and control of processes involving ionic liquid/H_2O mixtures.

Keywords Ioncell^{TM} · Ionic liquid · Raman spectroscopy · Chemometrics

Introduction

Ioncell^{TM} is a new process for the production of lyocell-type man-made cellulosic fibers based on cellulose pulp dissolution in an ionic liquid (IL), dry-jet wet spinning of the solution (spinning dope) in a water (H_2O) bath and a subsequent solvent recovery step, in which the IL and H_2O are separated. The whole process is operated in a closed loop system (Michud et al. 2016).

The Ioncell^{TM} process runs on non-imidazolium based protic ILs, among which [DBNH][OAc] has shown high potential for the production of strong cellulose fibers with minimal cellulose degradation (Parviainen et al. 2015; Michud et al. 2016; Kakko et al. 2017).

The acid-to-base molar ratio in the IL (A:B ratio) and the H_2O content in IL/H_2O mixtures are critical parameters for the cellulose dissolution and cellulose dope spinning. Water as a non-solvent can hinder the cellulose dissolution if its concentration in the IL/H_2O mixtures reaches a certain limit (usually few percent). Acetic acid acts also as a non-solvent if it is in excess compared to the base and prevent a good cellulose dissolution. In addition, the presence of water in the cellulose dope can affect the spinning by modifying the rheological properties of the dope (water acts as a softener). The A:B ratio and H_2O contents can vary substantially inside the process loop. For instance, H_2O concentration will decrease gradually between

Electronic supplementary material The online version of this article (https://doi.org/10.1007/s10570-019-02809-y) contains supplementary material, which is available to authorized users.

C. Guizani (✉) · S. Hellstén · J. Witos · H. Sixta
Department of Bioproducts and Biosystems, Aalto University, P. O. Box 16300, FI-00076, Espoo 02150, Finland
e-mail: chamseddine.guizani@aalto.fi

the spinning bath and the solvent recovery/purification steps. Also, the A:B ratio may change because of different acid and base vapor pressures or due to reactive azeotrope formation during recovery/purification steps using for instance evaporation and distillation (Kakko et al. 2017; Canongia Lopes and Rebelo 2010; Ahmad et al. 2016). To insure a good process stability and a homogenous fibers quality, those parameters should be well adjusted in each unit operation. Therefore, their fast and quantitative monitoring is an important part of the process control.

Ex-situ analytical techniques such as High Performance Liquid Chromatography (HPLC), Ion Chromatography (IC), Capillary Electrophoresis (CE) can be used to determine the anion or cation concentrations, while Nuclear Magnetic Resonance (NMR) spectroscopy can be used to determine the A:B ratio. The H_2O concentration in IL/H_2O mixtures can be determined by Karl Fisher (KF) titration (Parviainen et al. 2015; Ahmad et al. 2016).

The determination of H_2O concentration in IL/H_2O mixtures utilizing Refractive Index (RI) measurement is a simple and robust method for on-line analysis in a continuous process. However, this method is not sensitive to A:B ratio variation in IL/H_2O mixtures (results not shown). On top of that, many of the methods cited above are time consuming and tedious, and not suitable for process on-line analysis.

The development of fast, quantitative online analytical methods for the simultaneous determination of H_2O concentration and A:B ratio in IL/H_2O mixtures can benefit an increasing number of emerging processes based on IL/H_2O mixtures, for example, in biomass fractionation, pulp upgrading, or protein separation (Kohno and Ohno 2012; Sciarini et al. 2015; Stepan et al. 2016a, b).

Vibrational spectroscopy methods have the big advantages of being fast, non-destructive, and requiring much less efforts and time for sample preparation. In addition to the classical KF titration method as well as to various electrochemical methods (Wippermann et al. 2018; García-Mendoza and Aguilar 2015), vibrational spectroscopy excels in detecting and analyzing water contained in ILs. For instance, Viell and Marquardt (2012) developed a quantitative method for the determination of the composition of binary mixtures of water and various ILs using mid-infrared (mid-IR) spectroscopy. Also, Near-infrared (NIR) spectroscopy was successfully used for the non-invasive and in situ determination of concentrations and the structure of water absorbed by room-temperature ILs (Tran et al. 2015).

Raman spectroscopy is a well-known vibrational spectroscopy technique, based on the inelastic scattering of the light by a material. The proportional relationship between Raman scattering intensity and analyte concentration is the basis for most of the quantitative analysis done using Raman spectroscopy in gaseous, liquid, or solid samples (Pelletier 2003). In addition, Raman spectroscopy is also well suited for quantitative analysis of multiple components in a sample because a single Raman spectrum often contains enough information to determine their concentration simultaneously (Svensson et al. 1999). The use of Raman probes and optical fibers also allows remote monitoring of processes in hostile environments, which makes the technique very suitable for on-line analysis.

Raman spectroscopy has been widely used for the investigation of the intermolecular interactions, structures, and band assignment in pure ILs and mixtures of ILs (Berg 2007; Paschoal et al. 2017; Satyen et al. 2015). Nevertheless, methods for quantitative measurements of concentrations in IL/H_2O mixtures are scarcely investigated in the literature.

In this paper, we discuss the potential of Raman spectroscopy combined with univariate and multivariate calibrations for the fast and quantitative determination of H_2O, acid, and base contents in a wide and process-relevant range of H_2O/IL mixtures. The focus of the present work is on [DBNH][OAc]/H_2O mixtures.

Materials and methods

Materials

Samples of 1.5-Diazabicyclo[4.3.0]non-5-ene (DBN) (CAS no. 3001-72-7; purity $\geq$ 99.0% in mass) and acetic acid (HOAc) (CAS no. 64-19-7; purity $\geq$ 99.8% in mass) were purchased from Fluorochem and Sigma-Aldrich, respectively, and were used without further purification.

Sample preparation

Water-free ILs

[DBNH][OAc] was prepared by the slow and controlled addition of an equimolar amount of HOAc to DBN. The mixture was stirred and cooled in the beginning at 25 °C to divert the exothermic reaction enthalpy. When approaching the equimolar amounts in the mixture, the system was heated at 70 °C to avoid the crystallization of the IL. The system was kept for another hour at this temperature under mixing to ensure the reaction runs until completion. The water content of the synthesized IL is lower than 0.5 wt.%.

This IL sample was analyzed by ^{1}H NMR to determine its A:B ratio. The other samples were prepared by mixing the initial IL with known amounts of HOAc or DBN to reach the target A:B ratio. These samples were then mixed for homogenization and analyzed again by ^{1}H NMR for final determination of A:B ratio. The prepared samples were in the A:B molar ratio range of 0.4–1.98.

IL/H_2O mixtures

IL/H_2O mixtures were prepared by dilution of the water-free IL samples with water. A 1 mg precision electronic scale was used during the dilution process to adjust the IL/H_2O mixture to the target concentration. The covered IL concentration range was large enough to simulate concentrated and diluted samples (1.25–90 wt.% of IL in IL/H_2O mixtures) with different molar A:B ratios (0.4–1.98). The IL/H_2O mixtures were divided into calibration and validation sets for the model calibration and validation procedures. As each sample can be represented by its A:B ratio and IL concentration, the sample subsets are shown in Fig. 1.

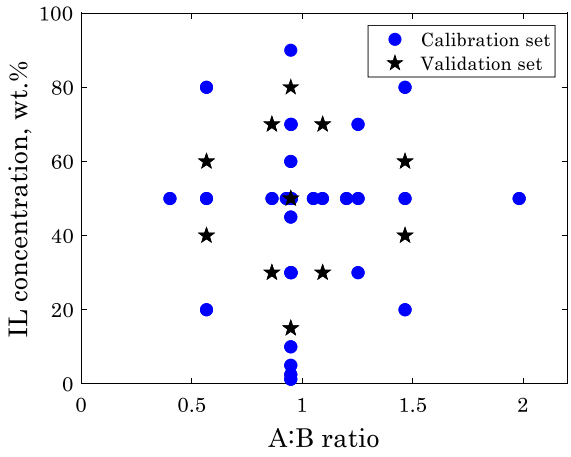

Fig. 1 Samples of IL/H_2O mixtures

^{1}H NMR measurements

Water-free IL samples were characterized by ^{1}H NMR. Samples were loaded into standard 5 mm diameter NMR tube and dissolved in DMSO-d6. The spectra were acquired at 23 °C using a Bruker 400 MHz Ultra Shield NMR spectrometer (Billerica, Massachusetts, USA). NMR spectra were collected following the standard zg30 sequence with eight transients and an acquisition time of 2.56 s. All of the spectra are referenced to tetramethylsilane. The ACD/1D NMR Processor software was used for the treatment of the raw data. The A:B ratios were calculated by considering the ratio between the area of peaks related to the acid and to the base, respectively.

Raman spectra acquisition

The samples were analyzed with an Alpha 300 R confocal Raman microscope (Witec GmbH, Germany) at ambient conditions. Nearly 100 µL of the IL/H_2O mixture were spread on a microscope concavity slide and covered with a cover glass. The Raman spectra were obtained by using a frequency doubled Nd:YAG laser (532.35 nm) at a constant power of 30 mW, and a Nikon 20x (NA = 0.4) air objective. The Raman system was equipped with a DU970 N-BV EMCCD camera behind a 600 lines/mm grating. The excitation laser was polarized horizontally. After fixing the focus using the microscopy mode, each single spectrum was acquired as an average of 32 scans with an integration time of 0.1 s/scan. The baseline of the spectra were corrected with WiTec Project 1.94 (WiTec GmbH, Germany) using a 2nd order polynomial equation.

In total, 75 spectra were collected, with at least two replicates for each sample. The calibration set comprises 54 spectra and the validation set comprises 21. The samples and spectra of the two sets were prepared and collected independently on different days.

Calibration methods development
for the determination of the acid, base, and H_2O concentration in the IL/H_2O mixtures

Univariate calibration

Univariate calibration is the simplest approach to build a quantitative calibration model. It is based on finding relationships between single Raman spectral variables (peak intensity, peak area, peak shift) and the analyte concentration. A Matlab® (The Mathworks, Inc. Natick, Massachusetts, United States) routine was created for the Raman spectra analysis, correlation identification and calculation of the calibration models parameters.

The fit quality is assessed through the coefficient of determination (R^2) and the Root Mean Square Error of Calibration (RMSEC) and Prediction (RMSEP) which are expressed as:$RMSEC = \sqrt{\frac{\sum_{i=1}^{N}\left(y_i^{cal}-\hat{y}_i^{cal}\right)^2}{N}}$, where y_i^{cal} and $\hat{y}_i^{cal}$ denote the measured and predicted values, respectively, and N the number of samples in the calibration data set, and$RMSEP = \sqrt{\frac{\sum_{i=1}^{K}\left(y_i^{val}-\hat{y}_i^{val}\right)^2}{K}}$,where y_i^{val} and $\hat{y}_i^{val}$ denoted the measured and predicted values, respectively, and K the number of samples in the validation data set.

Although univariate calibration can work successfully in some cases, it sometimes fails in giving good results when dealing with complex Raman spectra that show for instance overlapping bands or unexpected shifts over the calibration range. In those cases, a multivariate approach would be more appropriate for calibration model building (Geladi 2003; Geladi et al. 2004).

Multivariate calibration: Partial Least Squares regression (PLS)

When building calibration models using spectroscopic data and multivariate analysis, one usually encounters two main problems: there are typically much more spectral variables than samples, and there is a high variable collinearity encountered in most of the spectral data. This makes classical multiple linear regression (MLR) based on the original spectral variables either impossible or highly unstable.

A robust alternative to MLR is PLS regression. PLS projects data (spectral intensities in our case) in a new space with a smaller number of new variables. Those new variables are called components or Latent Variables (LVs). PLS calculates the LVs in a way that the covariance between the X block (spectral intensities), and the Y block (concentration of the different species) is maximized.

The LVs are mutually orthogonal, which suppresses problems related to matrix inversion when calculating the model coefficients. The reduction of the space dimension in addition to the mutual orthogonality of the LV makes PLS especially suitable for building predictive models out of spectroscopic data. A very good explanation of the principles of PLS is given in reference (Geladi and Kowalski 1986).

During the calibration procedure, the collected spectra are placed as rows in a X matrix (independent block), with n rows and k columns. Each row represents a spectrum and each column a single wavelength. The variables that we aim to predict are placed in a Y matrix (dependent block), with n rows and m columns. Each row represents one sample and each column a single variable.

Briefly, in PLS there are outer relations for which the X and Y blocks are decomposed into scores and loadings matrices:

$$X = TP' + E$$

$$Y = UQ' + F^*$$

where

- T and U represent respectively the score matrices for the X and Y blocks.
- P' and Q' represent respectively the loading matrices for the X and Y blocks.
- E and F^* represent respectively the matrices of residuals for the X and Y blocks after the projection onto a defined number of LV.

There is also an inner relation between the scores, linking both blocks

$$U = BT$$

where $\boldsymbol{B}$ is the matrix containing the regression vectors. A mixed relation can be written as:

$$Y = TBQ + F$$

where $\|F\|$ is to be minimized.

This mixed relation ensures the ability to use the model parameters for future prediction from a test set.

In the present study, the *X* block contains the Raman spectra of each sample and the *Y* block the weight fractions of acid, base, and H_2O in each sample.

The number of LVs, the fit quality, and model validation were investigated through the evaluation of the R^2 coefficient, RMSEC, and RMSEP.

Data analysis and model building were performed with Matlab® and the Matlab® PLS Toolbox (Eigenvector Research, Inc. Manson, United States) software packages.

Results and discussion

^{1}H NMR of water-free IL samples

The NMR spectra of the water-free ILs as well as the corresponding A:B ratio are shown in Fig. 2. The DMSO-d_6 singlet is visible at ≈ 2.5 ppm. The singlet observed in the range of ≈ 1.6–1.75 ppm corresponds to the protons of the methyl groups in the acetic acid/acetate molecules. The rest of the multiplets correspond to the different protons of the base and its protonated form. Details about the acid and base proton chemical shifts are indicated in the Figs. 1 and 2 of the electronic supplementary information (ESI).

As expected, only mixed peaks can be observed instead of peaks that represent molecular and ionic species separately. For the rapid exchange system, the observed ^{1}H chemical shift is assumed to be the weighted average of the molecular and ionic species.

One can notice a shift of the different peaks related to HOAc, DBN, and their ionized forms to the high ppm values when increasing the A:B ratio. These shifts can be directly linked to the different shielding/deshielding effects experienced by the protons when changing the A:B ratio.

For instance, when the A:B ratio is increased, protons belonging to the acid methyl group (1.6–1.8 ppm) are shifted downfield. This is probably due to a higher hydrogen-bonding network between these protons and the oxygen atoms of the carboxylate group in neighboring free acetic acid molecules. This reduces the shielding around these protons and make them resonate at higher frequency.

The position of the methyl group singlet is linearly correlated to the A:B ratio, with a noticeable increase of the slope starting from A:B = 0.85 denoting higher proton deshielding beyond this value (see Fig. 2 in the ESI). Similar linear relationships and slope change over the investigated A:B range were found for the equivalent protons bonded to C3 and C9 in DBN/

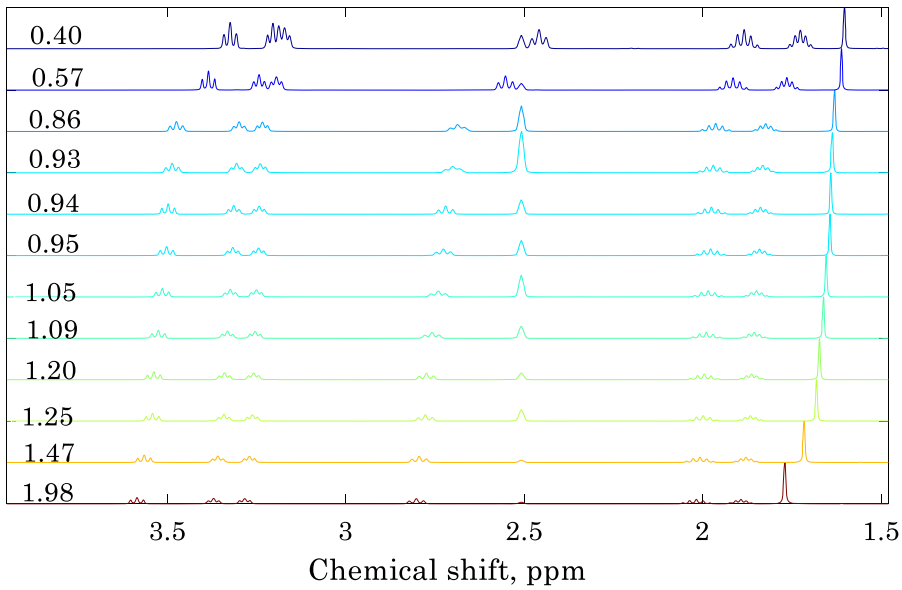

Fig. 2 NMR spectra of the water-free IL with different A:B ratios (A:B ratio is indicated on the left side of the figure for each sample)

$DBNH^+$. The change of slopes is, however, different. The slopes were pronounced below A:B = 1.1 and decreased markedly beyond this value, which means that the proton deshielding decreases significantly beyond this value. These results are also illustrated in the Fig. 2 in the ESI. The different chemical shifts can be used to calculate the IL ionicity as explained in this reference (Shen et al. 2017).

The A:B ratios were calculated by taking the ratio of the integral area of methyl group singlet (acid) to the sum of the integrated areas of the different multiplets (base). The area of the triplet observed in the range of ≈ 3.27–3.95 ppm, corresponding to the two hydrogen bonded to C9 was taken as a reference. The estimated relative error for the calculation of the A:B ratio was less than 5%.

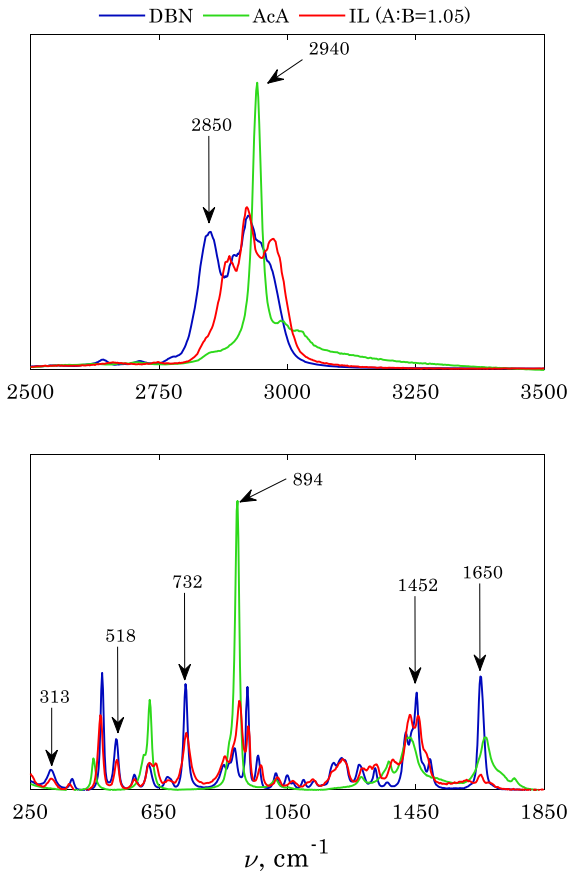

Fig. 3 Raman spectra of DBN, HOAc and the water-free ILs (A:B = 1.05). The spectra are divided into fingerprint region (down) and high frequency region (top) for the sake of clarity

Raman spectroscopy

Raman spectra of the acid, base, and IL

The area normalized Raman spectra of DBN, HOAc and IL (A:B = 1.05) are presented in Fig. 3. In the HOAc spectra, the two prominent peaks at ≈ 895 cm^{-1} and ≈ 2950 cm^{-1} are ascribed, respectively, to the C–C and C–H stretching vibrations. The medium intensity band at ≈ 1665 cm^{-1} is attributable to the C=O stretching vibration (Nakabayashi et al. 1999).

To the best of our knowledge, the assignment of the specific Raman bands for DBN has not been presented in the literature. The band assignment herein is based on Raman spectral tables (Smith and Dent 2004; Larkin 2011). The peak at 313 cm^{-1} and 518 cm^{-1} are likely to be C–N–C bending/deformation modes. The peak 732 cm^{-1} originates most probably from C–C vibrations. The peak at 1650 cm^{-1} could be ascribed to C=N stretching, while the peaks at 1452 cm^{-1} and 2850 cm^{-1} would be attributed to CH_2 vibrations. Interestingly, the peaks at 313 cm^{-1}, 518 cm^{-1}, and 732 cm^{-1} do not overlap with peaks of HOAc, and would probably be good candidates to build a calibration model.

The Raman spectra of IL (A:B = 1.05) display a complex pattern in which we can distinguish some features from the spectra of HOAc and DBN, respectively. One can note, for instance, that the peaks at 313, 518, and 732 cm^{-1} show a decrease in intensity compared to the pure base without any noticeable change in the shape or in the peak position, which confirms again their potential use for calibration. Some other overlapping peaks, for instance between 800–1000 cm^{-1} or between 2800–3200 cm^{-1}, are more complex to interpret and results from the overlaps/shifts of the peaks from HOAc and DBN. A noticeable shift of the DBN peak related to $–CH_2$ vibrations from 2850 cm^{-1} in the pure base to 2880 cm^{-1} in the IL is observed. Ionization and interactions between the molecular and ionized HOAc and DBN are probably behind those shifts.

Raman spectra of water-free A/B mixture with excess of base or acid

Figure 4 shows the Raman spectra of the IL in nearly equimolar amounts of acid and base and in an excess

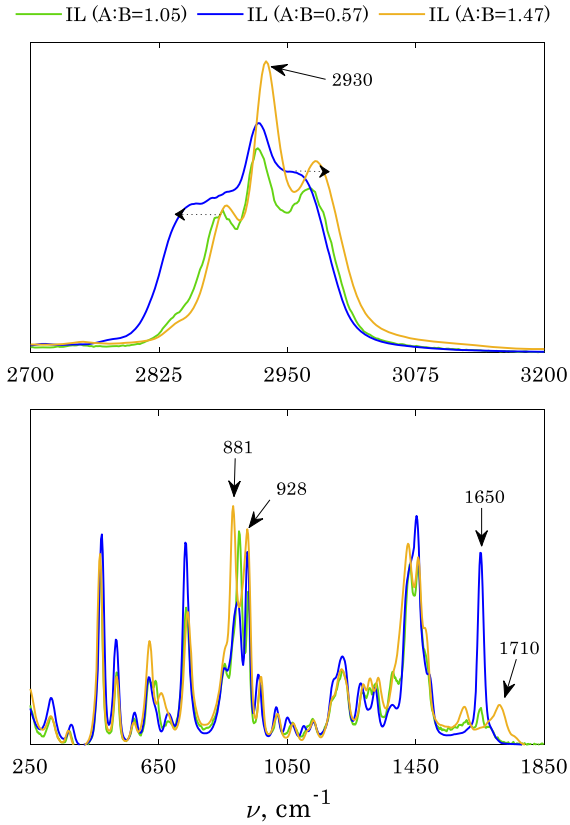

Fig. 4 Raman spectra of water-free IL with different A:B ratios. The spectra are divided into fingerprint region (down) and high frequency region (top) for the sake of clarity

of base or acid. In the fingerprint region, we can see noticeable changes in the spectra as a function of the A:B ratio. For instance, the peak at 899 cm^{-1} in the nearly equimolar IL shifts down to 881 cm^{-1} and becomes prominent compared to neighboring peaks when the acid is in excess, while it decreases markedly when the base is in excess. We already mentioned that the 1650 cm^{-1} peak intensities in the HOAc and DBN spectra decreased drastically in the nearly equimolar IL. When deviating from the equimolar composition, we can observe that the 1650 cm^{-1} peak intensity increases substantially when there is an excess of DBN, while in excess of HOAc, we can notice the presence of a peak at around 1710 cm^{-1}. Based on those observations, we can claim with a greater confidence that these peaks are related to the C=N and C=O vibrations in the non-ionized DBN (excess of base) and HOAc (excess of acid) forms.

Indeed, for the nearly equimolar composition, once the proton exchange occurs when the acid and base are mixed, a great proportion of the molecules become ionized, the two double bonds become delocalized, and no "real" C=O or C=N vibration can be seen in the Raman spectra of the IL. When there is an excess of acid or base, those bands are more prominent due the presence of the neutral molecules.

It is also worth-mentioning here that in the case of protic IL like [DBNH][OAc], a chemical equilibrium takes place between ionized and neutral species (the equilibrium constant is directly linked to the so called ionicity of the IL). This may then explain why the band intensities of the double bonds do not vanish completely even in nearly equimolar composition (presence of neutral species) (Canongia Lopes and Rebelo 2010).

The excess of base or acid in the mixtures affects also the spectrum in the high wave number region (2200–3200 cm^{-1}). At low A:B ratio (excess base), the peak at around 2900 cm^{-1} shifts to 2855 cm^{-1}, and the area in the range 2800–2900 cm^{-1} increases consequently. This shift most probably relates to the molecular vibrations in the free base. At a high A:B ratio of 1.47 (excess acid), the peak at around 2970 cm^{-1} shifts to 2980 cm^{-1}, the area in the range 2980-3150 cm^{-1} increases, and the 2930 cm^{-1} peak intensity increases markedly relatively to the adjacent peaks. Those changes are related to the presence of the molecular acid (see Fig. 3 for acetic acid peaks).

Effect of water on the Raman spectra of ILs as a function of the A:B ratio

So far, we showed that an excess of acid or base induces noticeable changes in the Raman spectra of A/B mixtures. In this section, we discuss the effect of water dilution of IL. The spectra of the different A:B ratio water-diluted IL samples (50 wt.% of water) are shown in Fig. 5.

Dilution with water caused indeed noticeable changes in the Raman spectra compared to the water-free ILs. A broad band ascribed to the different O–H stretch modes of the water molecules appeared in the wave number range of 3000–3700 cm^{-1}, in addition to another peak ascribed to a bending vibration mode of free water molecules near to 1595 cm^{-1} (Sun 2009). The peak at around 1650 cm^{-1} attributed to the C=N vibration in the free base drastically decreased in the presence of water (probably due to ionization) and is only visible for samples with low A:B ratios. The

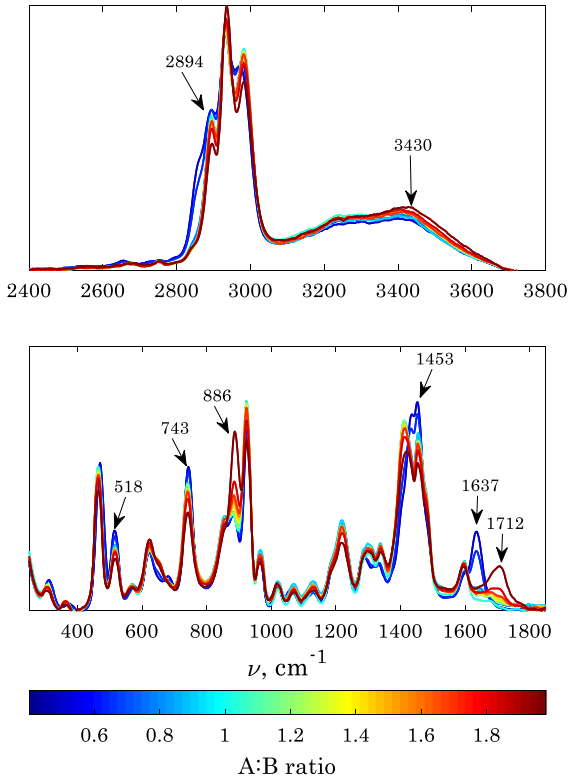

Fig. 5 Area-normalized Raman spectra of the 50 wt.% water diluted IL samples. The spectra are divided into fingerprint region (down) and high frequency region (top) for the sake of clarity. The color code is related to the A:B ratio (the reader can refer to the online version for the colors)

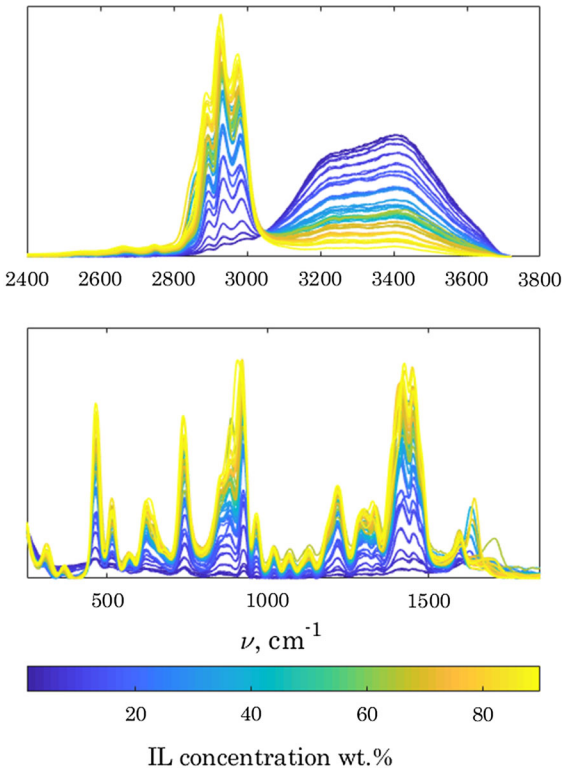

Fig. 6 Area-normalized Raman spectra of the different IL/H_2O solutions. The color code reflects the IL concentration in the IL/H_2O mixture. The spectra are divided into fingerprint region (down) and high frequency region (top) for the sake of clarity

peaks at 1600 cm^{-1} and 1700 cm^{-1} related to the free acid molecules are also visible in diluted samples with high A:B ratios. Here also, chemical equilibria define the ionization extent of the different molecules.

Drastic changes were also reported for the IR and NMR spectra of imidazolium-based ionic liquids having different anions upon the introduction of water due to interactions between the IL and H_2O molecules (Cha et al. 2014).

Raman spectra of the IL/water mixtures

The Raman spectra of the different IL/H_2O samples are shown in Fig. 6. As depicted in this figure, the intensity of the broad peak in the wavenumber range of 3000–3700 cm^{-1} ascribed to the different O–H vibrations modes in the water molecules increased with the dilution factor, while the scattering intensity from the acid and base molecules/ions in the IL (practically all the remaining spectral bands) decreased. This was expected since the Raman scattering intensity is proportional the concentration of the scattering molecules.

Although the presence of water caused noticeable changes in the Raman spectra of IL, its scattering does not noticeably interfere with the scattering resulting from the IL molecules. The water bending mode peak ($\sim$ 1640 cm^{-1}) interferes with the Raman bands of the IL. However, the water bending-mode peak intensity is relatively low compared to the intensities of the IL bands, and should not represent and obstacle to build a predictive quantitative model. A comparison of the spectra of water and a mixture of 50 wt.% IL(1.05:1)/50 wt.% H_2O at equal laser intensity is shown in the Fig. 4 in the ESI.

Univariate calibration approach for the determination of H_2O concentration in IL/H_2O mixtures

To predict the H_2O concentration in a H_2O/IL mixture, the intensity variation in the range of 2200–3800 cm^{-1} can be exploited. Although there is a small overlap between the peaks ascribed to IL and H_2O in the 3000–3200 cm^{-1} region, the respective signals are still relatively well separated.

We developed a quite simple method for the calibration. In our spectral treatment procedure, the spectral range was first narrowed to the 2200–3800 cm^{-1} region. The raw spectra were then area-normalized. The peak areas related to IL and H_2O are defined as follows:

$$IL_{peak\,area} = \int_{2200}^{3010} Idv$$

$$H_2O_{peak\,area} = \int_{3010}^{3800} Idv$$

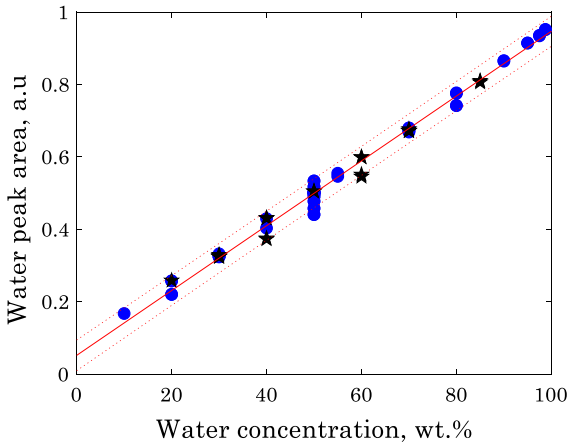

Fig. 7 Integral area of the Raman scattering intensity in the 3010-3800 cm^{-1} region vs water concentration. Blue circles: calibration data set. Black stars: validation data set. Solid lines: calibration model. Dashed lines: 95% confidence interval limits

The graphical representation of the H_2O peak area $H_2O_{peak\,area}$ as a function of the H_2O concentration is shown in Fig. 7.

A significant linear relationship is obtained between $H_2O_{peak\,area}$ and the H_2O mass fraction in the IL/H_2O mixture. Some discrepancies at equivalent H_2O mass fraction are observed for samples with different A:B ratios. Indeed, some of the spectral features change in the 2200–3010 cm^{-1} region, especially at low and high A:B ratios as discussed previously. These variations can be seen specifically for the samples with 50 wt.% of water, were the covered A:B range was the largest one.

Altogether, these changes do not dramatically affect the model. The RMSEC and RMSEP were 2.234 wt.% and 2.257 wt.%, respectively. These values are reasonable, considering the simple procedure and the large concentration range from 10 wt.% to 98.75 wt.% of H_2O content. The prediction error is comparable that reported by Viell and Marquardt (2012) who quantified H_2O in H_2O/IL mixtures using mid-infrared (mid-IR) spectroscopy using advanced spectral treatment methods. The prediction error reported in their study was lower than 2.3 wt.% over the entire concentration range. Models parameters and fit quality metrics for the prediction of the base concentration in IL/H_2O mixtures are given in Table 1.

Univariate calibration approach for the determination of the base concentration in IL/H_2O mixtures

The Raman scattering intensity from the IL components (acid and base) increases with IL concentration in the IL/H_2O mixtures as depicted in Fig. 6. Some peak intensities showed very good correlations with the base concentration, specifically those at 743 cm^{-1} and 2890 cm^{-1}. The intensities of these peaks as a function of the base concentration in the IL/H_2O mixture are depicted in Fig. 8.

Table 1 Models parameters and fit quality metrics for the prediction of the water concentration in IL/H_2O mixtures

Raman peak range, cm^{-1}	R^2	RMSEC, water wt.%	RMSEP, water wt.%	Model: $f(x) = ax + b$	
				a	b
3010-3800	0.991	2.234	2.257	0.008976 (0.008734, 0.009218)	0.05309 (0.03843, 0.06774)

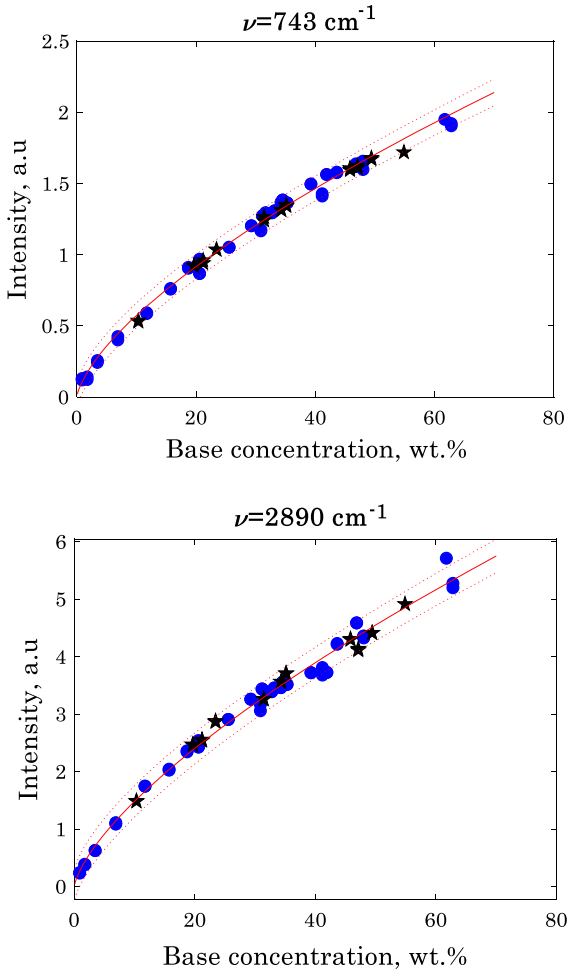

Fig. 8 Evolution of peak intensities at 743 cm^{-1} and 2890 cm^{-1} as a function of the base concentration in the IL/H_2O mixtures. Blue circles: calibration data set. Black stars: validation data set. Solid lines: calibration model. Dashed lines: 95% confidence interval limits

The relationship between the peak intensities and the base concentration is, however, not linear. The reasons behind this non-linearity over the base concentration range are not clear. Polynomial models can be used to approximate a complex nonlinear relationship, as they are just the Taylor series expansion of the unknown nonlinear function. However, we found that the observed relationships could be well described with simple power law models, which we adopted for the calibration equation.

As depicted in Fig. 8, the fit quality is relatively good over the covered base concentration range for the two peaks. The model parameters and the fit quality metrics (R^2, RMSEC, and RMSEP) for the prediction of the base concentration in IL/H_2O mixtures are given in Table 2.

For both peaks, the RMSEC and RMSEP were lower than 2 wt.%, which is again a quite reasonable value regarding the covered range. Nevertheless, using the peak at 2890 cm^{-1} would result in a better model sensitivity, as the intensity range is larger over the same covered base concentration range.

So far, the univariate calibration showed a good potential for the quantification of water and base in IL/H_2O mixtures. Nevertheless, it showed also limitations, as we were not able to predict the acid concentration in the IL/H_2O mixtures using single spectral features. The acid concentration can be still obtained by difference to 100% assuming that only water, acid, and base are present in the solution.

Using multivariate calibration can greatly improve the calibration model quality and performance, as it utilizes all the information in the spectra and not only focuses on a single variable. In the next section, we will discuss the potential of one of the multivariate calibration methods, namely the PLS regression.

PLS regression for the simultaneous determination of the IL components and H_2O content in IL/H_2O mixtures

Preprocessing is a very important step when performing multivariate data analysis. In our attempts to build the PLS calibration model, we tested several spectra preprocessing methods and evaluated them in the light

Table 2 Models parameters and fit quality metrics for the prediction of the base concentration in IL/H_2O mixtures

Raman shift, cm^{-1}	R^2	RMSEC, Base wt.%	RMSEP, Base wt.%	Model: $f(x) = ax^b$	
				a	b
743	0.991	1.566	1.086	0.1209 (0.1101, 0.1317)	0.6763 (0.6517, 0.7008)
2890	0.985	1.944	1.840	0.2992 (0.2673, 0.3311)	0.6957 (0.6665, 0.725)

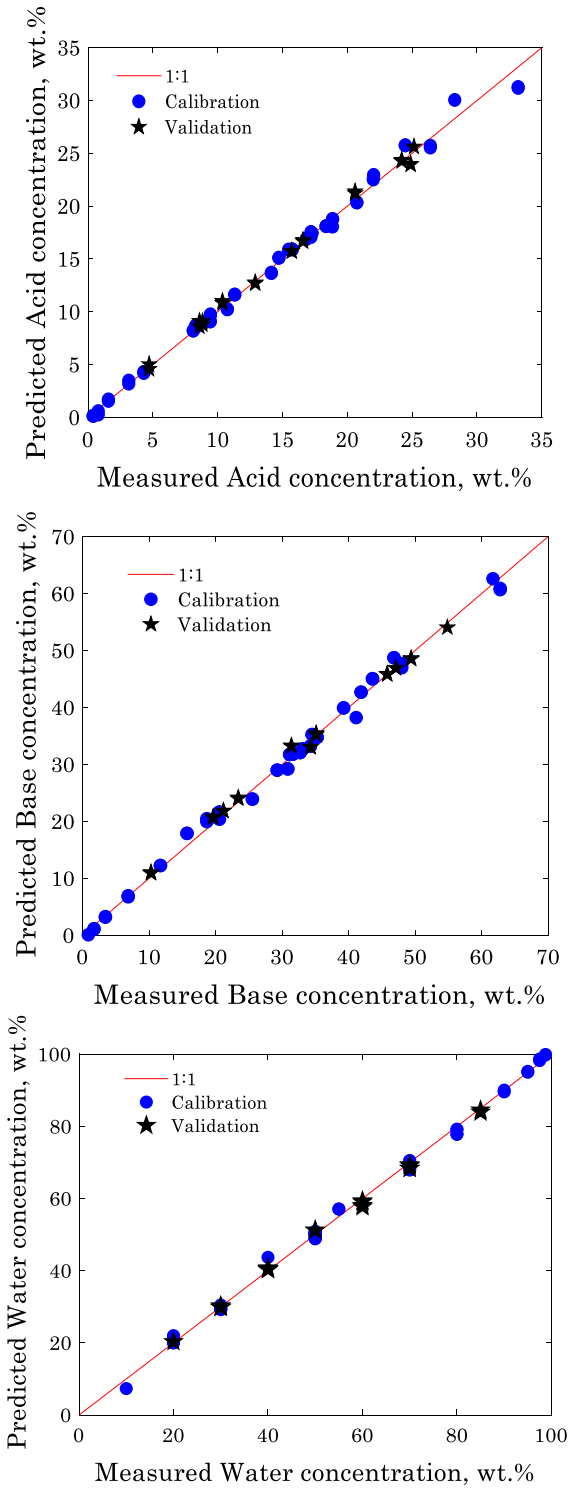

Fig. 9 Prediction vs measurements plots for the acid, base, and H_2O concentrations in the H_2O/IL mixtures

of the model fit quality. The retained preprocessing strategy includes baseline correction, smoothing (10 points moving window), area normalization and mean centering of the raw spectra (*X* block). The *Y* block data were mean centered.

The number of the model LVs was selected based on the minimization of the RMSECV and a visual inspection of the LVs. A model with four LVs leads to a very good fitting with more than 99% of explained variance in both *X* and *Y* blocks.

The measured and predicted values of acid, base, and H_2O concentrations for the calibration and validation data sets are shown in Fig. 9. The reader can see that the different data points are well distributed around the y = x line for both sets, which reflects a good model fit quality.

The PLS calibration approach was clearly successful in predicting simultaneously the acid, base, and H_2O contents in IL/H_2O mixtures. The PLS model statistics are shown in Table 3.

The RMSEs are reasonable regarding the relatively wide covered range for the three variables. It has to be noted that some of the validation set samples have acid, base, and H_2O concentrations from the calibration set samples, which also reflects a good model prediction ability

Those results are, to the authors' best knowledge, the first in the literature to show the potential of Raman spectroscopy in combination with chemometrics for a fast and quantitative determination of the Il components and H_2O contents in IL/H_2O mixtures. The applicability of this method can be extended to a wider range of processes involving IL/H_2O mixtures (Kohno and Ohno 2012; Sciarini et al. 2015; Stepan et al. 2016a, b).

Discussion on the PLS calibration model

The percent variance captured by the PLS regression model for the *X* and *Y* blocks are given in Table 4. LV 1 and LV 2 explain already nearly 99% of the variance in the data. The latent variable LV 1 explains the greatest part of the variance, respectively 96.53% and 93.14% in the *X* and *Y* blocks.

The score plot based on the two first LVs as well as the loadings plots for the four LVs are shown in Fig. 10. The scores represent the coordinates of the samples in the new LV space. Samples having similar scores on the same LV are similar regarding to this

Table 3 PLS model statistics for the prediction of acid, base, and H_2O contents in the H_2O/IL mixtures

	Base (wt.%)	Acid (wt.%)	Water (wt.%)
Concentration range	0.86–62.81	0.39–33.17	10-97.75
RMSEC, wt.%	1.137	0.634	1.175
RMSEP, wt.%	0.908	0.441	1.037
R^2 Calibration	0.995	0.994	0.997
R^2 Prediction	0.996	0.996	0.998

Table 4 Percent variance captured by the PLS regression model

Latent variable (LV)	*X*-Block explained variance (%)	*Y*-Block explained variance (%)
1	96.53	93.14
2	2.31	2.86
3	0.53	3.24
4	0.38	0.40

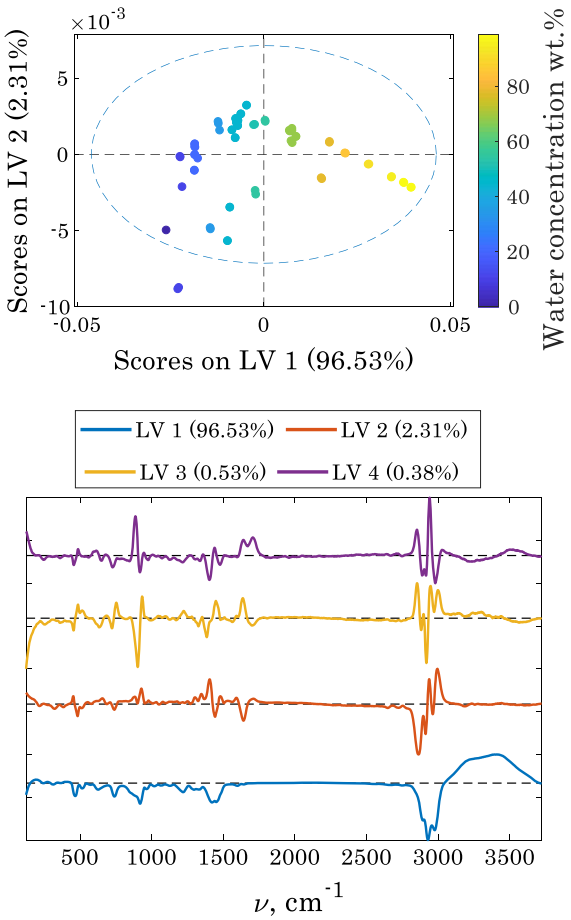

Fig. 10 Score plot based on LV 1 and LV 2 (top) and loadings plots (bottom) for the four LVs

LV. The corresponding loadings are used to interpret what is causing the changes in the scores and can help to elucidate the physical meaning of a particular LV. A particular loading shows the spectral features responsible for the pattern in the score plot. A high loading value for a certain wavelength (or a range of wavelengths) means that this latter contributes highly in building the latent variable.

The positive peaks in the LV 1 loading spectrum show an almost complete signal of the water peak. The negative peaks constitute an almost reversed spectrum of a water-free IL. From our previous discussion, we can deduce that the LV 1 is mainly explaining variation of IL (respectively water) concentration in the mixture.

This observation is confirmed when looking at the LV 1-LV 2 score plot, where the scores are colored with water concentration in the mixture. The samples with IL concentration close to the mean concentration (around 40 wt.%) have a score value of zero because the data are mean centered. We can see that samples with negative scores on LV 1 have IL concentrations below this average, while samples with positive scores on LV1 have lower IL concentration than this average.

From the loading plot of LV 2, one can already see that this latent variable is not related to the H_2O concentration in the sample, since the loading values for LV 2 are close to zero in the wavenumber region corresponding to the O–H vibrations.

The LV 2 loadings show positive and negative peaks. A closer look reveals that the negative peaks corresponds to vibrational frequencies of chemical

bonds found in the base and the positive peaks occur at the vibrational frequencies of the acid (see previous discussion on peak assignment). This is confirmed on the score plot, where the samples were found to be separated along LV 2 according to the A:B ratio.

The same applies for LV 3 and LV 4 which would explain variation in the A:B ratio rather than concentration as the respective loadings showed features related to molecular vibrations in A and B. Both LVs would also explain in part the presence of molecular acid and/or base in the sample, as some of the spectral features related to them appear on the loadings plot.

Altogether, LV 2, LV 3 and LV 4 are related to the variation of A:B ratio in the mixture, while LV 1 explains the variation of IL concentration in it.

Conclusions

In this paper, we have shown that Raman spectroscopy in combination with univariate or multivariate calibration can be applied successfully for the quantitative analysis of protic IL components and H_2O in IL/H_2O mixtures. Compared to the univariate calibration, the multivariate calibration using PLS regression showed excellent performance for the quantitative analysis of the IL components and water over wide concentration ranges. These results suggest that the combination of Raman spectroscopy and chemometrics could be applied more universally to monitor and control a variety of processes involving the use of IL/H_2O mixtures.

Acknowledgments Open access funding provided by Aalto University. The authors gratefully thank Dr. Mikko Mäkelä from the Department of Bioproducts and Biosystems in Aalto University for the fruitful conversations about multivariate data analysis and comments about the present work.

References

Ahmad W, Ostonen A, Jakobsson K et al (2016) Feasibility of thermal separation in recycling of the distillable ionic liquid [DBNH][OAc] in cellulose fiber production. Chem Eng Res Des 114:287–298. https://doi.org/10.1016/j.cherd.2016.08.032

Berg RW (2007) Raman spectroscopy and ab initio model calculations on ionic liquids. Monatshefte fur Chemie 138:1045–1075. https://doi.org/10.1007/s00706-007-0760-9

Canongia Lopes J, Rebelo LP (2010) Ionic liquids and reactive azeotropes: the continuity of the aprotic and protic classes. Phys Chem Chem Phys 12:1648. https://doi.org/10.1039/c001176m

Cha S, Ao M, Sung W et al (2014) Structures of ionic liquid-water mixtures investigated by IR and NMR spectroscopy. Phys Chem Chem Phys 16:9591–9601. https://doi.org/10.1039/c4cp00589a

García-Mendoza A, Aguilar JC (2015) Analysis of water in room temperature ionic liquids by linear sweep, differential pulse and square wave cathodic stripping voltammetries. Electrochim Acta 182:238–246. https://doi.org/10.1016/j.electacta.2015.09.045

Geladi P (2003) Chemometrics in spectroscopy. Part 1. Classical chemometrics. Spectrochim Acta Part B At Spectrosc 58:767–782. https://doi.org/10.1016/S0584-8547(03)00037-5

Geladi P, Kowalski BR (1986) Partial least-squares regression: a tutorial. Anal Chim Acta 185:1–17. https://doi.org/10.1016/0003-2670(86)80028-9

Geladi P, Sethson B, Nyström J et al (2004) Chemometrics in spectroscopy: part 2. Examples. Spectrochim Acta Part B At Spectrosc 59:1347–1357. https://doi.org/10.1016/j.sab.2004.06.009

Kakko T, King AWT, Kilpeläinen I (2017) Homogenous esterification of cellulose pulp in [DBNH][OAc]. Cellulose 24:5341–5354. https://doi.org/10.1007/s10570-017-1521-5

Kohno Y, Ohno H (2012) Ionic liquid/water mixtures: from hostility to conciliation. Chem Commun 48:7119–7130. https://doi.org/10.1039/c2cc31638b

Larkin P (2011) Infrared and Raman spectroscopy: principles and spectral interpretation. Elsevier, London

Michud A, Tanttu M, Asaadi S et al (2016) Ioncell-F: ionic liquid-based cellulosic textile fibers as an alternative to viscose and Lyocell. Text Res J 86:543–552. https://doi.org/10.1177/0040517515591774

Nakabayashi T, Kosugi K, Nishi N (1999) Liquid structure of acetic acid studied by Raman spectroscopy and Ab initio molecular orbital calculations. J Phys Chem A 103:8595–8603. https://doi.org/10.1021/jp991501d

Parviainen A, Wahlström R, Liimatainen U et al (2015) Sustainability of cellulose dissolution and regeneration in 1,5-diazabicyclo[4.3.0]non-5-enium acetate: a batch simulation of the IONCELL-F process. RSC Adv 5:69728–69737. https://doi.org/10.1039/c5ra12386k

Paschoal VH, Faria LFO, Ribeiro MCC (2017) Vibrational spectroscopy of ionic liquids. Chem Rev 117:7053–7112. https://doi.org/10.1021/acs.chemrev.6b00461

Pelletier MJ (2003) Quantitative analysis using Raman spectrometry. Appl Spectrosc 57:20A–42A

Satyen S, Hiroi T, Iwata K, Hamaguchi H (2015) Raman spectroscopy and the heterogeneous liquid structure in ionic liquids. In: Plechkova N V., Seddon KR (eds) Ionic

Liquids Completely UnCOILed: Critical Expert Overviews, pp 165–187

Sciarini LS, Rolland-Sabaté A, Guilois S et al (2015) Understanding the destructuration of starch in water-ionic liquid mixtures. Green Chem 17:291–299. https://doi.org/10.1039/c4gc01248h

Shen M, Zhang Y, Chen K et al (2017) Ionicity of protic ionic liquid: quantitative measurement by spectroscopic methods. J Phys Chem B 121:1372–1376. https://doi.org/10.1021/acs.jpcb.6b11624

Smith E, Dent G (2004) Modern Raman spectroscopy—a practical approach. Wiley, Chichester

Stepan AM, Michud A, Hellstén S et al (2016a) Ioncell-P&F: pulp fractionation and fiber spinning with ionic liquids. Ind Eng Chem Res 55:8225–8233. https://doi.org/10.1021/acs.iecr.6b00071

Stepan AM, Monshizadeh A, Hummel M et al (2016b) Cellulose fractionation with IONCELL-P. Carbohydr Polym 150:99–106. https://doi.org/10.1016/j.carbpol.2016.04.099

Sun Q (2009) The Raman OH stretching bands of liquid water. Vib Spectrosc 51:213–217. https://doi.org/10.1016/j.vibspec.2009.05.002

Svensson O, Josefson M, Langkilde FW (1999) Reaction monitoring using Raman spectroscopy and chemometrics. Chemom Intell Lab Syst 49:49–66. https://doi.org/10.1016/S0169-7439(99)00025-8

Tran CD, Silvia HLDP, Oliveira D (2015) Absorption of water by room-temperature ionic liquids: effect of anions on concentration and state of water. Appl Spectrosc 57:152–157. https://doi.org/10.18632/oncotarget.4514

Viell J, Marquardt W (2012) Concentration measurements in ionic liquid-water mixtures by mid-infrared spectroscopy and indirect hard modeling. Appl Spectrosc 66:208–217. https://doi.org/10.1366/11-06427

Wippermann K, Giffin J, Korte C (2018) In Situ determination of the water content of ionic liquids. J Electrochem Soc 165:H263–H270. https://doi.org/10.1149/2.0991805jes